ACS APPLIED MATERIALS & INTERFACES

www.acsami.org

Research Article

Tailoring the Nanostructure of Graphene as an Oil-Based Additive: toward Synergistic Lubrication with an Amorphous Carbon Film

Xiaowei Li,* Dekun Zhang,* Xiaowei Xu, and Kwang-Ryeol Lee*

Cite This: *ACS Appl. Mater. Interfaces* 2020, 12, 43320−43330

Read Online

ACCESS | Metrics & More | Article Recommendations | Supporting Information

ABSTRACT: Graphene exhibits great potential as a lubricant additive to enhance the antifriction capacity of moving mechanical components in synergism with amorphous carbon (a-C) as a solid lubricant. However, it is particularly challenging for experiments to accurately examine the friction dependence on the physical nanostructure of the graphene additive and the corresponding interfacial reactions because of the inevitable complexity of the graphene structure fabricated in experiments. Here, we address this puzzle regarding the coeffect of the size and content of the graphene additive at the a-C interface using reactive molecular dynamics simulations. Results reveal that the friction-reducing behavior is more sensitive to graphene size than content. For each graphene structure, with increasing content, the friction coefficient always decreases first and then increases, while the friction behavior exhibits significant dependence on the graphene size when the graphene content is fixed. In particular, the optimized size and content of the graphene additive are suggested, in which an excellent antifriction behavior or even superlubricity can be achieved. Analysis of the friction interface indicates that with increasing graphene size, the dominated low-friction mechanism transforms from the high mobilities of the base oil and graphene additive in synergism to the passivation and graphene-induced smoothing of the friction interface. These outcomes disclose the roadmap for developing a robust solid−liquid synergy lubricating system.

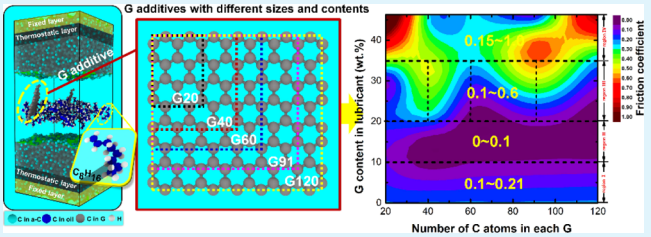

KEYWORDS: *graphene, lubricant additive, amorphous carbon, friction mechanism, reactive molecular dynamics*

1. INTRODUCTION

Graphene, a kind of 2-dimensional material with sp^2-bonded carbon atoms, attracts great academic and technical interests since it is discovered[1,2] because of its excellent mechanical, electronic, chemical inertness properties, and so on.[3,4] More importantly, it has been intensively used as an additive or dopant to endow the materials with enhanced or new properties.[5−11] For example, Chen et al.[8] reported that embedding well-dispersed graphene nanosheets into epoxy coating remarkably improved the anticorrosion performance and wear resistance properties. Fan and Wang[9] revealed that graphene not only possessed outstanding anti-irradiation capacity but also significantly improved the space performance and tribological properties of multialkylated cyclopentane fluids. Cao et al.[10] found that after 1300 cycles of discharging and charging at 22 C, the graphene-embedded $Li_4Ti_5O_{12}$ nanocomposite material showed ∼91% retention (101 mA hg^{-1}) of the initial capacity, which was far better than retentions recently reported for similar anode materials.

Recently, because of the aggravated energy and environment issues, it becomes urgent to develop an advanced lubricating system for minimizing the triboinduced energy dissipation, material losses, and CO_2 emissions that occurred in some critical moving components, such as the automotive engine.[12] The solid−liquid synergy lubricating technology,[13−16] which spins the liquid lubricant on solid lubricating films, has been proved to be an ideal choice for moving mechanical components. It can overcome the risk of cold welding of mated solid films, weaken the rupture of liquid lubricant, and also provide crucial protection under instantaneously harsh conditions of oil-starved or oil-free lubrication. In general, the liquid lubricant is composed of base oil and various modifier additives, while the graphene gains tremendous attention as a strong lubricant additive candidate. It can extremely enhance the antifriction performance of the liquid lubricant because of its lamellar structure following the weak intermolecular interaction[17,18] and thus reduces the frictional losses, consumed cumulative fuel mass by 17%, and exhaust emissions (CO_2, NO_x, and CO).[19,20] In particular, on the surface which has been coated by an amorphous carbon (a-C) film as one of the best solid lubricating candidates,[21−24] previous theoretical and experimental studies[15,25−28] revealed that a-C and graphene exhibited a synergistic effect on the improvement

Received: July 16, 2020
Accepted: August 27, 2020
Published: August 27, 2020

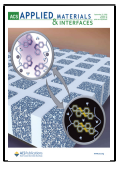

https://dx.doi.org/10.1021/acsami.0c12890
ACS Appl. Mater. Interfaces 2020, 12, 43320−43330

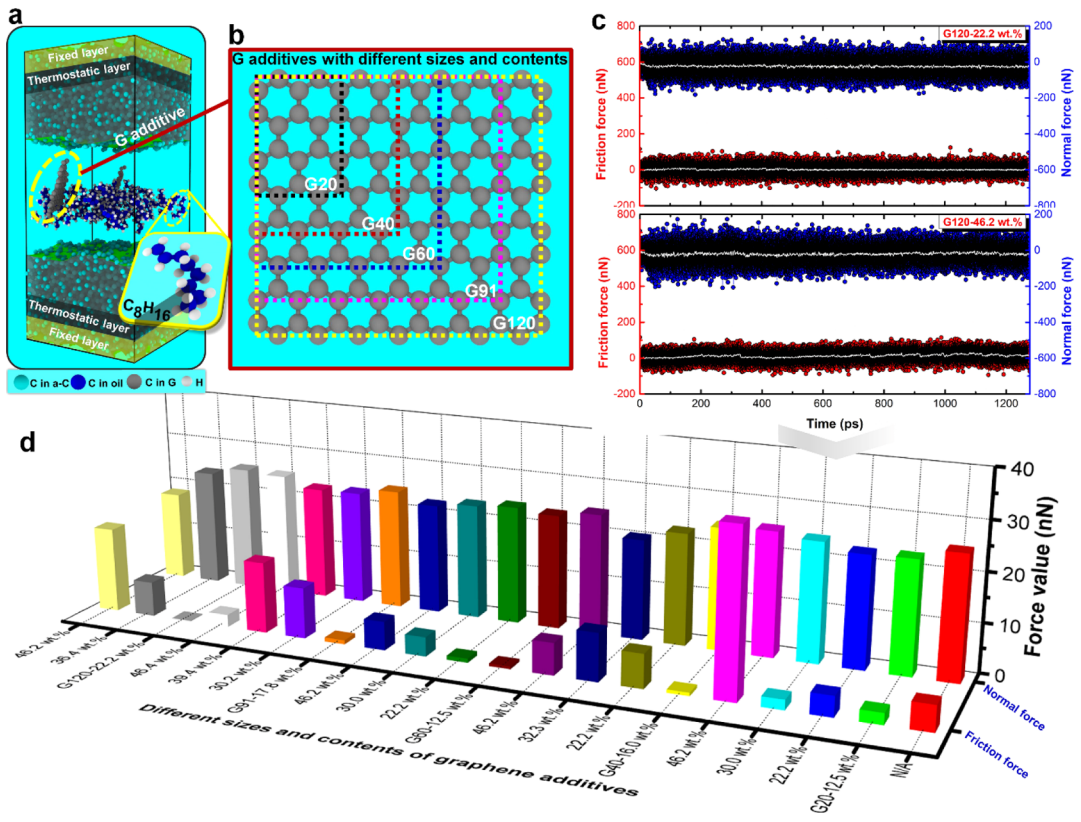

Figure 1. Friction model and friction results under different sizes and contents of G lubricant additives: (a) friction model composed of a-C, C_8H_{16} as a base oil, and the G fragment as the lubricant additive; (b) G fragments with different G sizes, abbreviated as G20−G120 according to the number of C atoms in each G structure for convenience; (c) friction curves including friction and normal forces with sliding time for the systems with G120−22.2 wt % and G120−46.2 wt %; and (d) average values of friction force and normal force during the steady-state friction stage for each case.

of the friction-reducing ability. For example, Li et al.[25] showed that compared with the pure base oil on the a-C surface, the graphene additive anchored to the a-C surface, forming a block physical protective film and thus resulting in the friction coefficient reduced by 90%. Wang et al.[27] reported that at a high applied load, the a-C film played the role of loading bearing, while the graphene additive could effectively improve the friction reduction and wear resistance via the formation of a thick tribofilm.

Although the graphene has been chemically or thermally exfoliated for application as a lubricant additive, it is inevitably accompanied by the presence of graphene fragments with different sizes, contents, layers, and interlayer spacings. He et al.[29] have clarified the influence of layers and interlayer spacing of graphene additives on the nanostructural evolution of the graphene additive and the formation of the interfacial transfer layer. However, because of this complexity and uncertainty of the graphene structure as a lubricant additive, it becomes inaccessible from an experimental approach to clearly and accurately distinguish the friction dependence on the size and corresponding content of the graphene additive. The transformation of the interfacial structure induced by the graphene additive and a-C also cannot be achieved in situ because of the limitation of experimental characterization, while it is a prerequisite for the development of a high-efficient liquid lubricant and advanced solid−liquid synergy lubricating system.

Considering this, we investigate the friction behavior of the a-C/lubricant system (Figure 1a) composited with graphene (G) as an additive and α-olefin (C_8H_{16}) as the base oil via the reactive molecular dynamics simulation (RMD). The size and content of the G additive are tailored, in which the G additives with different sizes are named as G20, G40, G60, G91, and G120 (Figure 1b) according to the number of C atoms in each structure. The dependence of the friction behavior and underlying mechanism on the size and content of the graphene additive is discussed systematically with regards to the transformation of the interfacial structure, physicochemical properties of the base oil and G additive, and the interaction between a-C, base oil, and the G additive. To the best of our knowledge, exploring the effect of different graphene additives on the a-C/lubricant system has not been reported yet. It is of fundamental interest to disclose the difference in the antifriction property and interfacial evolution caused by different graphene structures, which can provide a key point for the design of a carbon-based solid−liquid synergy lubricating system for applications.

2. METHODS

2.1. Model and Simulation Parameters. All RMD calculations were performed using the Large-scale Atomic/Molecular Massively Parallel Simulator code.[30] Similar to the previous study,[25] the "*sandwich*" model, consisting of a lower a-C substrate, liquid lubricant, and upper a-C counterface, was fabricated to simulate the friction system, as shown in Figure 1a. The a-C structure with a size of 42.88 × 40.36 × 31.00 Å^3 contained 6877 carbon atoms and its sp^3 fraction, sp^2 fraction, and density were 24 at. %, 72 at. %, and 2.7 g/cm^3, respectively. It was deposited by an atom-by-atom method.[31] The liquid lubricant consisted of linear alpha olefin, C_8H_{16}, as base oil[32]

https://dx.doi.org/10.1021/acsami.0c12890
ACS Appl. Mater. Interfaces 2020, 12, 43320−43330

and graphene structures with different sizes and contents as lubricant additives. For each case, the number of C_8H_{16} molecules was fixed at 45. In order to investigate the G-induced friction response of the a-C/lubricant system, the size of the G additive ranged from G20 to G120 (Figure 1b), corresponding to the number of C atoms increased from 20 to 120; the G content in the base oil changed from 0 to 46.2 wt %. The initial separation distance between the liquid lubricant and the lower or upper a-C film was 3 Å. Before the RMD simulation process, a three-layer assumption was applied to the a-C/lubricant/a-C system,[16,25] including a fixed layer (yellow background in Figure 1a) for imitating the semi-infinite system, a thermostatic layer (gray background in Figure 1a) for providing a thermal reservoir for the system by a constant temperature of 300 K using a microcanonical ensemble with a Berendsen thermostat,[33] and a free layer (remaining region including a-C and the lubricant in Figure 1a) for inspecting the mechano−chemical reactions of the friction interface. Besides, a time step of 0.25 fs was used and periodic boundary conditions were applied along the *x*- and *y*-directions. ReaxFF potential developed by Tavazza et al.,[34] which has been fully validated by our previous studies,[16,25,32,35,36] was adopted to describe the interaction between a-C and the liquid lubricant. The cutoff radius values for the C−C, C−H, and H−H bonding interactions were defined as 1.85 Å, 1.20 Å, and 0.85 Å, respectively.

2.2. Friction Simulation. During the simulation process, a three-step process was carried out step by step: (i) geometric optimization at 300 K for 2.5 ps; (ii) a loading process to achieve the specified value of contact pressure (5 GPa) during 25 ps; and (iii) a sliding process with constant contact pressure (5 GPa) and sliding velocity (10 m/s) along the *x*-direction for 1250 ps. It should be mentioned that although this contact pressure and sliding velocity were much higher than experimental values, our and other previous studies[14,16,36−40] have confirmed that they were appropriate for sufficiently sampling the phase space and examining the potential tribochemical reactions of the a-C film on an atomic scale. After the friction process, the friction coefficient (μ) was calculated as follows

$$\mu = \frac{f}{W} \tag{1}$$

where the frictional force, *f*, is calculated by summing the force acting on the fixed atoms of the lower a-C model along the sliding direction, and *W* is the normal force acting on the fixed atoms of the lower a-C model along the *z* direction. The forces acting on the sliding atoms were averaged every 100 MD steps, and thus, a total of 50,000 individual data points for the friction and normal forces were obtained during 5,000,000 MD steps.

3. RESULTS AND DISCUSSION

3.1. Friction Results under G Lubricant Additives with Different Sizes and Contents. Figure 1c shows the friction curves including friction and normal forces with sliding time for the systems with G120−22.2 wt % and G120−46.2 wt %. It can be seen that similar to the additive-free case,[32] introducing the different graphene additives into the friction interface does not affect the changes in friction and normal forces with sliding time, which exhibits no obvious running-in process. However, it still can be distinguished that the system with low G content can reach the steady-state friction stage more quickly than that with high G content. It should be mentioned that in the present work, only the low number of C atoms in the a-C structure (fixed layer of the bottom a-C substrate in Figure 1a) is adopted to sum the change in forces. This causes the strong sensitivity of instantaneous force values to the interfacial interaction, such as the stick-slip feature reported by Harrison,[41] and thus results in the large fluctuations in both the friction force and normal force during the sliding process, even the minus signals of forces.[16] However, it hardly affects the average values of both the friction and normal forces, which has been confirmed by previous studies.[37,42,43] In particular, these large fluctuations can be effectively eliminated by increasing the number of C atoms and the time interval (25 fs in this work) for each force statistics.

The friction and normal force values, which are generated during the last 200 ps of the steady-state sliding process (Figure 1c), are adopted to calculate the average friction force and normal force values, respectively, as shown in Figure 1d. It can be seen that the friction force with content or size of the G additive changes significantly, ranging from 0.13 to 33.64 nN, while the normal force evolves in a relatively small range from 18.33 to 25.62 nN. Hertzian theory describes the relationship between the contact pressure, real contact area, and normal force of the friction system.[44]

$$\sigma = \frac{W}{A} \tag{2}$$

where *W* is the applied normal force, *A* is the real contact area, and σ is the Hertzian contact pressure (5 GPa in this work). Hence, this change in normal force originates from the evolution of the real contact area with G structures, as confirmed by Figure S1 of the Supporting Information. In addition, the real contact area displays different dependences on G size and content. It tends to be increased with G size while decreased with G content, suggesting the differences in interactions between the lubricant and mating materials and the evolutions of interfacial structures, as will be discussed later.

3.2. Friction Coefficient with Size and Content of the G Additive. Figure 2 gives the change in the friction coefficient with size and content of the G additive. Note that for the additive-free case, the friction coefficient is 0.21, but after adding the graphene into C_8H_{16} base oil, the friction coefficient is more sensitive to the size than to the content of the G additive. When the G size is fixed, the friction coefficient tends to be decreased first and then increased with G content significantly, agreeing well with previous reports;[19,25] the low friction coefficient (<0.05) can be approximately achieved among the G content scale from 10 to 20 wt % for each G size. However, when the G content is fixed, there are different behaviors of the friction coefficient as a function of G size observed. This can be divided into four regions as follows according to the G content:

(i) Region I (0−10 wt %): the friction coefficient (0.1−0.21) shows no dependence on the G size.

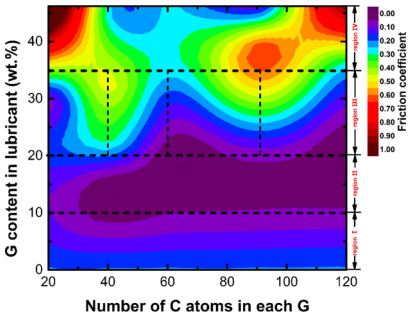

Figure 2. Change in the friction coefficient with size and content of the G additive.

https://dx.doi.org/10.1021/acsami.0c12890
ACS Appl. Mater. Interfaces 2020, 12, 43320−43330

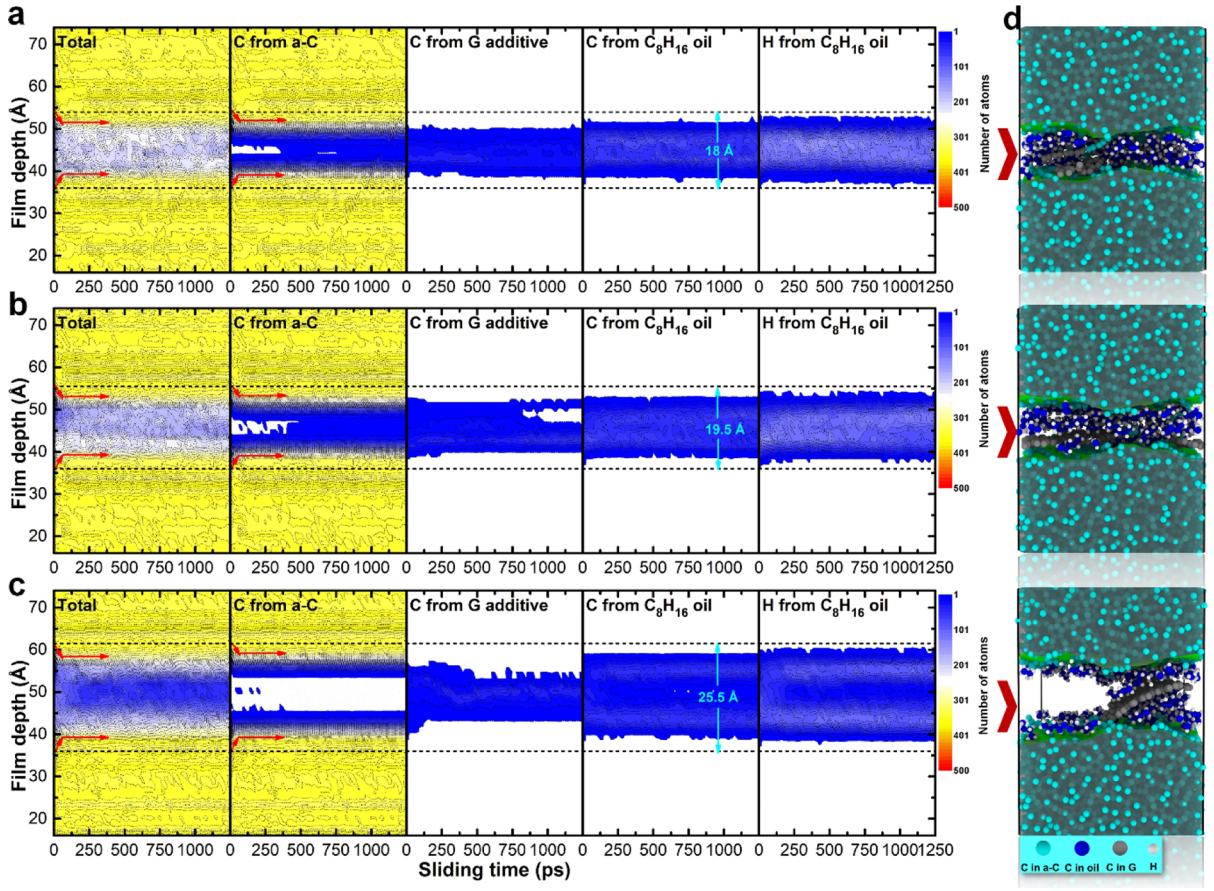

Figure 3. Depth profiles of atomic distribution in the system. (a–c) are the atomic distributions of C and H atoms vs sliding time in the system with a G size of G20, G60, and G120, respectively, when the G content is fixed at 22.2 wt %. (d) Corresponding morphology at a sliding time of 1250 ps for each case.

(ii) Region II (10–20 wt %): the friction coefficient with G size changes in the range of 0–0.1. It decreases first as G size changes from G20 to G40 and then becomes stable with G size further increased from G40 to G120.

(iii) Region III (20–35 wt %): the friction coefficient (0.1–0.6) shows a symmetric change with G size ranging from G20 to G60 or from G60 to G120. As the G size changes from G20 to G40, the friction coefficient increases from 0.1 to 0.5, while it decreases from 0.5 to 0.05 with further increasing G size to G60. A similar change is also observed in the range of G60–G120.

(iv) Region IV (>35 wt %): the friction coefficient (0.15–1) has no regular change with G size because of the complicated a-C/G and G/G interactions, but the systems normally exhibit a higher friction coefficient than the additive-free case.

These results indicate that for the G as an oil-based lubricant additive, both its size and content have a significant and complicated effect on the synergistic friction behavior of G with a-C and the base oil. It is well-known that the friction behavior is closely related to the structural transformation of the friction interface,[32,37,38,42,45] such as the hybridized structure, the interaction between a-C and the lubricant,[14,15,46] and the mobility of the base oil,[16,25] which can be activated by the triboinduced shearing or thermal effects. However, because of the low contact pressure, the heat generated at the friction interface can be dissipated into the thermal layer and the liquid lubricant, leading to the slight rise of interfacial temperature, as illustrated in Figure S2 of the Supporting Information. Hence, the structural properties of the friction interface are mainly affected by the shearing effect during the sliding process.

3.3. Depth Profiles of Atomic Distribution in the System Vs Sliding Time. In order to characterize the evolution of the interfacial structure caused by different sizes and contents of G additives, the atomic distributions of C and H atoms along the film depth direction are plotted first for each system, as given in Figures 3 and S3 of the Supporting Information, respectively. They can define the width of the friction interface as accurate as density and coordination distributions reported in previous work.[16] It can be seen that the width of the friction interface as a function of G size increases monotonously. Taking the G content of 22.2 wt % for example (Figure 3a–c), the interfacial width reaches 25.5 Å from 18.0 Å when the G size increases to G120 from G20. However, when the G size is fixed, the interfacial width with G content increases first and then decreases (Figure S3 of the Supporting Information).

Moreover, by the distributions of C atoms from both the a-C films and base oil, it can be obtained that following the increase in G size from G20 to G60 and G120, the oil molecules tend to be shifted to the positions close to two a-C surfaces and thus contribute to the complete separation of mated a-C surfaces against cold welding (Figure 3c,d). This is in consistence with Moseler's study.[14] Although this behavior is also observed for the system as a function of G content (Figure S3 of the Supporting Information), the enhanced chemical bonding

https://dx.doi.org/10.1021/acsami.0c12890
ACS Appl. Mater. Interfaces 2020, 12, 43320–43330

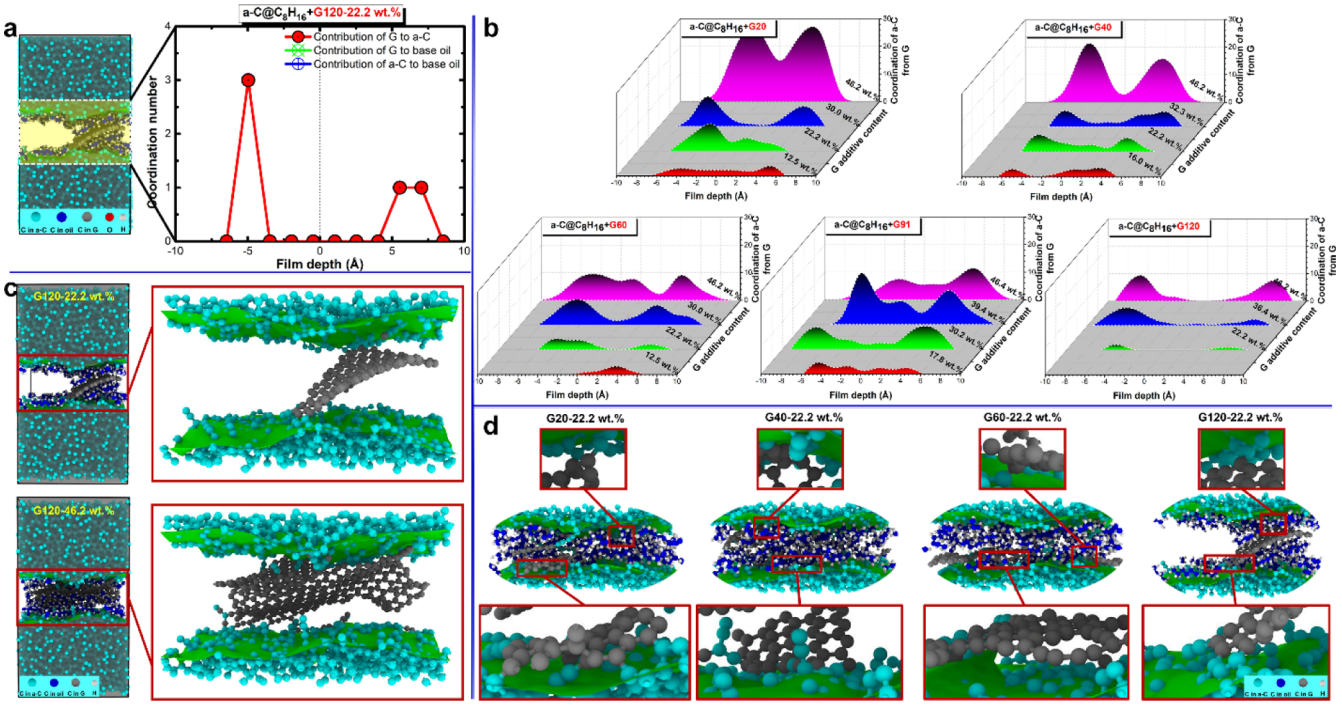

Figure 4. Interaction between the a-C, base oil, and G additive. (a) Coordination number contribution between the a-C, base oil, and G additive for the a-C@C_8H_{16} + G120−22.2 wt % system after the sliding process. (b) Coordination number distribution of a-C after a sliding time of 1250 ps, which is contributed by th eG additive only for each case. (c) Morphologies of friction interfaces for the a-C@C_8H_{16} + G120 systems with G contents of 22.2 wt % and 46.2 wt % after a sliding time of 1250 ps. (d) Morphologies of friction interfaces for the systems with G20, G40, G60, and G120 as lubricant additives a after sliding time of 1250 ps, in which the G content is fixed at 22.2 wt % for each case.

between G fragments and mated a-C surfaces will also have a negative effect on the sliding of the friction interface. Especially for the H atoms in the base oil, they are deviated from central to two side positions of the friction interface with size or content of the G additive, close to the a-C surfaces (Figures 3d and S3 of the Supporting Information), which is favorable to the sliding of the friction interface, as will be discussed later.

Furthermore, according to the distribution of C atoms from different G additives, most of the G additives with different sizes and contents are distributed at the whole interface (Figure 3) rather than firmly localized at one a-C surface as a protective film or tribofilm.[25,47,48] However, the different number of C atoms from the G additive exists at the two a-C/G interfaces, suggesting the different binding behaviors. In addition, Figures 3 and S3 of the Supporting Information also indicate that the friction-induced change in structural properties mainly occurs at the composite interface rather than at the intrinsic a-C film, which should be taken to explore the change in the friction behavior with sizes and contents of G additives.

3.4. Interaction between the a-C, Base Oil, and G Additive. Using the defined region of the friction interface in Figures 3 and S3 of the Supporting Information, the interaction between the a-C, base oil, and G additive is evaluated. Taking the a-C@C_8H_{16} + G120−22.2 wt % system for example (Figure 4a), the base oil makes no contribution to the coordination number of the a-C and G additive. This suggests the intermolecular interaction between the base oil and the a-C or G additive without any chemical bonding, which is in agreement with our previous study.[25] However, the chemical interaction occurs between the a-C and G additive because of the binding of G side atoms with the reactive sites on the a-C surface, as confirmed by Figure 4a.

Figure 4b further shows the coordination number distribution of a-C contributed by the G additive only for each case. Note that for each G structure, the contribution of G to the coordination number of a-C increases obviously with G content, suggesting the enhanced cross-linking interaction between G and two a-C counter surfaces, as confirmed by the results in Figure 4c. It not only prevents the friction interface from sliding but also causes the rupture of the G structure step by step under the shearing effect. This behavior is similar to that in the previous report, in which an unsaturated organic modifier concurrently chemisorbed on both a-C surfaces following the severe decomposition.[14] Besides, because of the increased content, the piling up and self-mated interaction of G fragments are also observed for each case. This increases interfacial roughness and also accounts for the change in interfacial width with G content (Figure S3 of the Supporting Information), consistent with the previous study.[25]

However, under the same G content, such as 22.2 wt %, the coordination number of a-C contributed by the G additive decreases with G size (Figure 4b). This is because the G additive with a small size has a higher ratio of the edge atoms to the nonedge atoms and higher mobility than the large one, which is more reactive and easier to interact with a-C dangling bonds (Figure 4d). Most importantly, it is also contributed by the enhanced mechanical and supporting role of G structures as a function of G size, which can resist the effect of the normal load. This prohibits the further interaction of G with a-C and also the presence of cold welding between mated a-C surfaces (Figure 4d), which coincides with the result in Figure 3. In addition, note that with the increase in G size, the base oil molecules tend to be localized around the graphene additive rather than uniform distribution, suggesting the improved load-

https://dx.doi.org/10.1021/acsami.0c12890
ACS Appl. Mater. Interfaces 2020, 12, 43320−43330

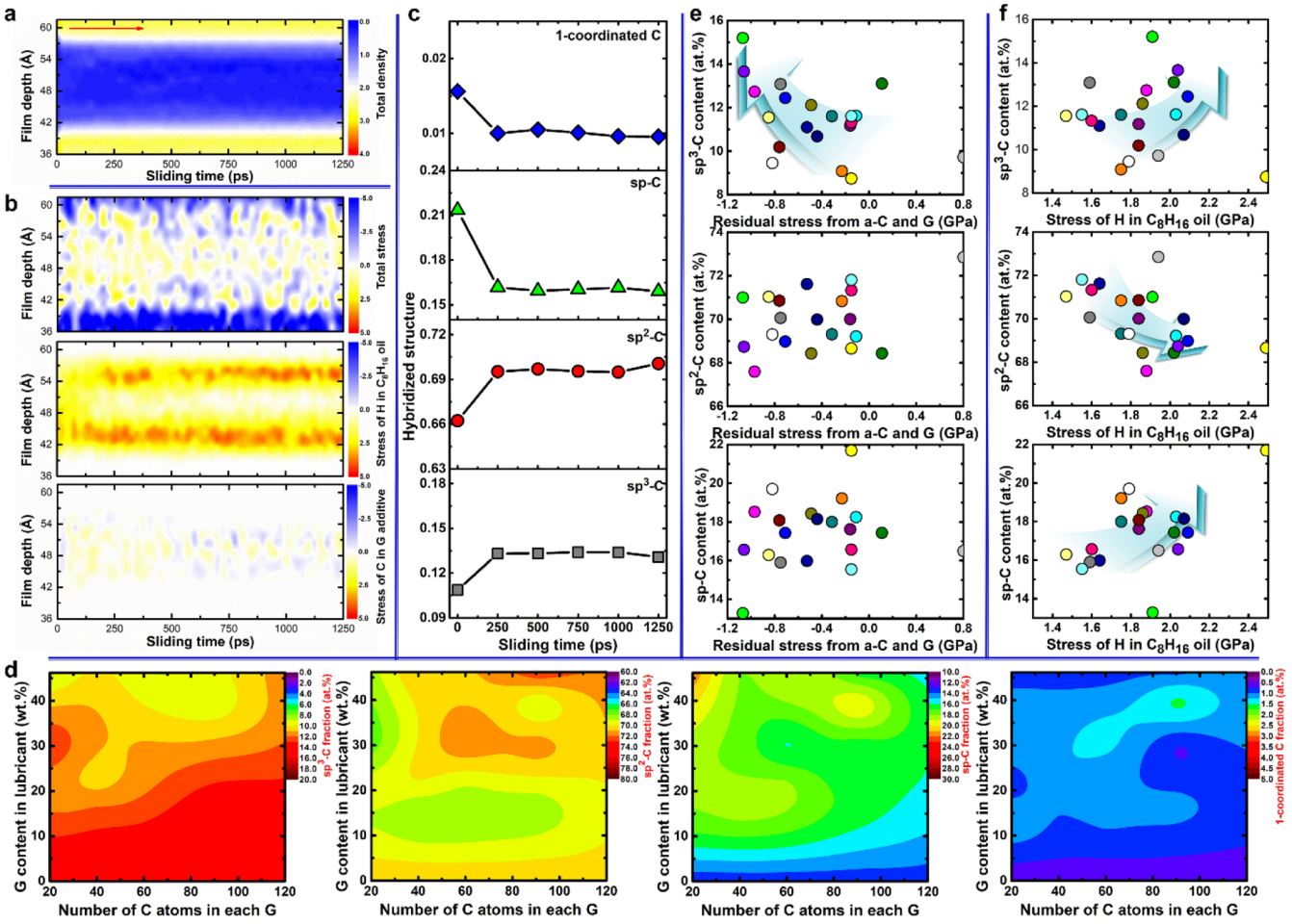

Figure 5. Evolution of structural properties of the friction interface with size and content of the G additive. (a) Total density, (b) stress (total, G, and C_8H_{16} oil), and (c) hybridized structure of C atoms at the friction interface as a function of sliding time for the a-C@C_8H_{16} + G120−22.2 wt % system. (d) Hybridized structure of the friction interface with size and content of the G additive. Relationship between the hybridized structure and residual stress of (e) a-C + G or (f) H in C_8H_{16} oil at the friction interface. Note that in (c−f), only the contributions of both the a-C and G to the hybridized structure are considered because of the existing chemical bonding.

carrying capacity[50,51] and thus contributing to the increase in interfacial width, as shown in Figure 3.

Especially, in Figure 4b,c, it can be seen that for the system with an extremely low friction coefficient, such as a-C@C_8H_{16} + G120−22.2 wt %, the two mated a-C surfaces show different binding strengths with the G additive: one having a strong chemical binding and the other having a weak bonding state with G side atoms. For the a-C@C_8H_{16} + G60−12.5 wt % (Figure S4 of the Supporting Information), it even only chemisorbs to one of the two contacting surfaces, named as "anchoring", to smooth the sliding interface.[14,25] Conversely, the concurrently strong anchoring, named as "cross-linking", of the G additive with both the a-C counter surfaces will not only result in the fragmentation of the G additive, which agrees with Moseler's report,[14] but also affect the mobility of base oil molecules following the increased resistance of the sliding interface. In addition, Figure 4b also reveals that in some systems, the coordination distribution of a-C contributed by the G additive is even located at the middle region of the friction interface, implying the serious chemical interaction of a-C with the G additive and thus potentially affecting the mobility of base oils.

3.5. Transformation of Structural Properties of the Friction Interface with Sliding Time. First, for all friction systems, they exhibit similar behaviors for the changes in density and residual stress with sliding time. Taking the a-C@C_8H_{16} + G120−22.2 wt % system for example (Figure 5a), it can be seen that the total density of the friction interface increases first during the short running-in process because of the increased number of C atoms from a-C (Figure S5 of the Supporting Information), and then, it becomes stable to reach the steady-state stage. This is similar to the additive-free case reported by our previous study.[32] Figure 5b shows the distribution of total stress at the friction interface. Note that it has no regular change with sliding time, but the tensile stress exists in the middle region of the friction interface, corresponding to the repulsive force.[42,49] This mainly originates from the H atoms in C_8H_{16} base oils,[16,25] as confirmed by Figure 5b, but the C atoms in the G additive also make a slight contribution to the tensile stress at the friction interface because of the triboinduced shearing effect.

The transformation of the carbon hybridized structure of the friction interface is illustrated in Figure 5c, in which only the contribution from both the a-C and G additive is considered because of the absence of chemical bonding between the base oil and the a-C or G additive. First, note that a relatively high sp-C fraction existed because the friction interface is mainly composed of two a-C surfaces (Figure 3) without any

https://dx.doi.org/10.1021/acsami.0c12890
ACS Appl. Mater. Interfaces 2020, 12, 43320−43330

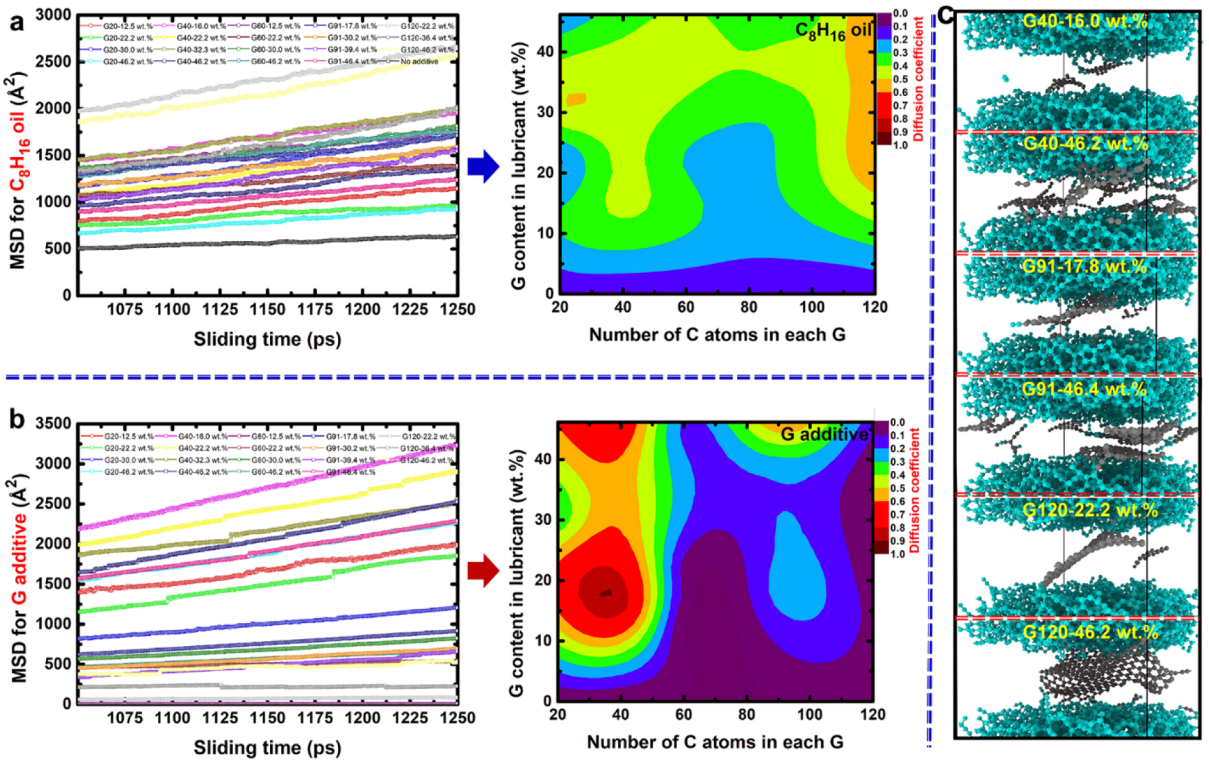

Figure 6. Effect of size and content of the G additive on the mobility of base oil. (a,b) are the MSD curves and fitted diffusion coefficients of the C_8H_{16} base oil and G additive, respectively. (c) Interfacial structure of the systems with different sizes and contents of G additives, in which the base oil molecules are neglected for view.

contamination as observed in the experiment. For each system, during the sliding process, the sp^3-C and sp^2-C fractions of the friction interface increase first, which is accompanied by the decrease in both the sp-C and 1-coordinated carbon fractions, and then reach the stable values. This interfacial reconstruction is related to the tribochemical reactions within the a-C films[52] and the rebonding of G or its dissociated fragments with the a-C surface.[25,46] However, most importantly, it is due to the H atoms in C_8H_{16} close to the a-C surface with high repulsive forces (Figure 5b), not only promoting the passivation of a-C dangling bonds[25,49] but also the sliding of the friction interface, especially the mobility of base oil molecules.

3.6. Effect of Size and Content of the G Additive on the Structure of the Friction Interface. In order to explore the dependence of the friction coefficient on the G structure, after a sliding time of 1250 ps, we further analyze the change in the interfacial structure and density with size and content of the G additive, as shown in Figures 5d and S6 of the Supporting Information, respectively. In general, when the G size is fixed, the density of the friction interface with G content decreases slightly, which is similar to its change with G size (Figure S6 of the Supporting Information). They are related to the change in interfacial width, as confirmed by Figures 3 and S3 of the Supporting Information.

Because C_8H_{16} base oil molecules have no chemical bonding with both the a-C and G additive, the hybridized structure of the friction interface, which is contributed by both the a-C and G additive only, is analyzed. Figure 5d gives the change in the hybridized structure (sp^3-C, sp^2-C, and sp-C) of the friction interface with size and content of the G additive. According to the divided regions in Figure 2, it can be obtained as follows:

(i) Region I (0−10 wt %): the hybridized structure with G size almost has no change.

(ii) Region II (10−20 wt %): both the sp^3-C and sp^2-C fractions increase slightly following the decrease in sp-C and 1-coordinated carbon hybridized structures. This should make contributions to the drop of the friction coefficient, as illustrated in Figure 2.

(iii) Region III (20−35 wt %): the hybridized structure shows strong sensitivity to the G size. The sp^3-C fraction decreases from G20 to G40 and then increases, while the sp^2-C fraction increases first from G20 to G60 and then decreases from G60 to G120. The complicated transformation of the hybridized structure suggests the aggravated G/G and G/a-C interactions.

(iv) Region IV (>35 wt %): when the G content increases to larger than 35 at. %, there is even no regular change in the hybridized structure with G size.

Moreover, for the system with a fixed G size, the fraction of sp-hybridized dangling bonds increases as the content increases from 0 to 46.2 at. %. This is due to the presence of cross-linking between G and mated a-C surfaces, inducing the serious dissociation of the G structure. In addition, it will roughen the friction interface and also increase the intermolecular interaction and possibility of cross-linking formation between G and a-C surfaces,[25] resulting in the increase in the friction coefficient.

For the change in the hybridized structure, previous studies demonstrated that it is seriously related to the stress state of a-C, G, and H in C_8H_{16} molecules at the friction interface.[25,32,38,42,49] Figure 5e shows the relationship between the stress and hybridized structure of the friction interface, in which the contributions of base oil to stress and hybridization

https://dx.doi.org/10.1021/acsami.0c12890
ACS Appl. Mater. Interfaces 2020, 12, 43320−43330

are neglected. It reveals that the increase in compressive stress of the friction interface causes the transformation of the hybridized structure from sp-C and sp^2-C to sp^3-C, which is consistent with the *P-T* phase diagram.[38] In addition, the repulsive force of H atoms from C_8H_{16} also induces the sp^2-to-sp^3 transformation, but it is also accompanied by the increased sp-C fraction, as shown in Figure 5f. However, because of the low contact pressure,[16,25] the rise of flash temperature at the friction interface is very low (Figure S2 of the Supporting Information), so the thermal activation of interfacial hybridized reactions is negligible (Figure S7 of the Supporting Information). Besides the main contributions from the stress and temperature, the transformation of the hybridized structure can be also affected by the differences in the locally normal force, the interfacial roughness, the chemical interaction between the G additive or its fragments and a-C, and the intermolecular interaction between a-C or G and base oil, which leads to the presence of the discrete data points in Figure 5e,f, respectively.

3.7. Effect of Size and Content of the G Additive on the Mobility of Base Oil. The mean square displacements (MSDs) for both the G additive and C_8H_{16} base oil are estimated separately using the following equation,[53] which is an essential tool to evaluate the effect of the mobility of the liquid lubricant on the friction property.

$$\mathrm{MSD} = r^2(t) = \frac{1}{N}\sum_{i=1}^{N} |r_i(t) - r_i(0)|^2 \tag{3}$$

$$\mathrm{MSD} = 6Dt \tag{4}$$

where N is the number of i atoms in the system and $r_i(t)$ and $r_i(0)$ are the positions of the ith atom at time t and 0, respectively. The MSD values generated during the last 200 ps are used to fit the diffusion coefficient of the C_8H_{16} base oil and G additive, respectively, for each case, as illustrated in Figure 6a,b. First, it can be seen that under the fixed G content, the system with a small G size, such as G20 and G40, normally shows higher mobilities of both the G and C_8H_{16} base oil than that with a large G size, such as G60 and G91. However, as the G size increases to G120, the G additive and C_8H_{16} exhibit the contrary changes in the diffusion coefficient with G size. In particular, the diffusion coefficient of the G additive displays strong dependence on the size and content of the G additive. This is related to the interaction between a-C and the G additive at the friction interface, which also significantly affects the mobility of C_8H_{16} base oil.

As the G size is fixed in the system, the mobility of C_8H_{16} base oil as a function of G content increases gradually (Figure 6a). On one hand, this results from the increase in undissociated G content, which can more effectively smooth the a-C surface as a protective film and shield the intermolecular interaction of a-C dangling bonds to base oil molecules (such as G120−46.2 wt % in Figure 6c).[25,47,48] On the other hand, this is related to the enhanced cross-linking of G with both a-C surfaces. Although this cross-linking is accompanied by the increased shearing resistance during the sliding process (Figure 4b,c), it can play a key role in increasing the width of the friction interface (Figure S3 of the Supporting Information) and also resist most of the applied normal force. This suggests the improved load-bearing capacity of base oil, as confirmed by previous studies.[50,51]

However, the change in the mobility of the G additive with G content (Figure 6b) is more sensitive to the G size than that of C_8H_{16} oil, including:

- When the G size is small (<G60), the mobility of the G additive with its content ranging from 0 to 20 wt % increases quickly, showing a synergistic effect with base oil to improve the friction behavior. This originates from the anchoring effect of the small G structure to different a-C surfaces (such as G40−16.0 wt % in Figure 6c). On further increasing the G content from 20 wt % to 46.2 wt %, the self-bonding between G additives and the cross-linking of G with a-C surfaces occur.[25] Combined with the serious friction-induced dissociation of the G structure (such as G40−46.2 wt % in Figure 6c), these account for the slight decrease in the G diffusion coefficient.
- As the G size is further increased to the one smaller than G120, the mechanical property of the G additive is highly improved. Under the high G content (>20 wt %), although the cross-linking of G with both the a-C surfaces is also aggravated, G structures can adsorb on different a-C surfaces (such as G91−46.4 wt % in Figure 6c), leading to the increase in the diffusion coefficient. However, under the low G content (<20 wt %), the G additive almost has no movement. This is because they can strongly anchor to one a-C surface as a protective film to smooth the surface (such as G91−17.8 wt % in Figure 6c) and improve the friction behavior significantly.[25,27,47]
- As the G size is G120, it also stably anchors to one a-C surface as a protective film and thus there is no diffusion behavior of the G additive observed (such as G120−22.2 wt % in Figure 6c). Especially, G120 highly smooths the sliding interface and also strengthens the load-bearing property of C_8H_{16} oil,[50,51] which are further improved with increasing the G120 content (such as G120−46.2 wt % in Figure 6c), contributing to the increase in the diffusion coefficient of C_8H_{16} base oil.

3.8. Discussion on the Underlying Friction Mechanism. It is well-known that the friction behavior is strongly related to the structure of the friction interface and the hydrodynamic lubrication of the liquid lubricant including base oil and additives.[13−16,21,25,38,49] The friction mechanism of the a-C/lubricant system with size and content of the G additive is discussed, according to the abovementioned analysis.

First, for the system with a fixed G size, the friction coefficient with G content decreases first and then increases (Figure 2), as proved by previous experimental and simulation reports.[19,25] When the G content is smaller than 20 wt %, the G additive shows high mobility because of the friction-induced dissociation (<G60) or anchors to one a-C as a protective film to smooth the surface instead of mobility (Figure 6b).[25,27] Combined with the relatively low fraction of dangling bonds at the friction interface (Figure 5d), these can account for the low friction coefficient observed in Figure 2. By increasing the G content to more than 20 wt %, the enhanced cross-linking of the G additive with two a-C counter surfaces and the piling up of the G structure occur (Figure 6c). The existence of G-induced cross-linking can support the applied load to improve the hydrodynamic lubrication of base oil (Figure 6a).[50,51] However, it significantly increases the sliding resistance of mated a-C surfaces because of the covalent bonding. In

https://dx.doi.org/10.1021/acsami.0c12890
ACS Appl. Mater. Interfaces 2020, 12, 43320−43330

addition, it also causes the partial dissociation of the G structure and thus increases the sp-C dangling bonds at the friction interface (Figure 5d), aggravating the adhesive interactions.[41,52] Hence, the cross-linking and increased fraction of unsaturated atoms mainly result in the high friction coefficient (Figure 2).

The change in the friction coefficient with G size exhibits different behaviors when the G content ranges from 0 to 46.2 wt %. In region I (0−10 wt %, Figure 2), the interfacial structure (Figure 5d) and the diffusion coefficient of base oil (Figure 6a) are almost independent of the G size. However, the mobility of the G additive with size decreases slightly (Figure 6b) because of the different interactions between a-C and the G additive. When the G size is small, the high mobilities of the G additive and base oil improve the friction coefficient in synergism. However, when the G size is large, such as G60, the G can serve as a protective film to reduce the friction coefficient.[25,27,47] However, compared with the additive-free case, because of the low G content, it plays a limited role in reducing the friction coefficient which has no change with G size, as illustrated in Figure 2.

In region II (10−20 wt %, Figure 2), as the G size increases from G20 to G40, the G additive and C_8H_{16} base oil exhibit high mobilities (Figure 6). However, because of the weak mechanical property of G, its structure is ruptured because of the shearing effect following the high fraction of sp-C dangling bonds at the interface (Figure 5d). On further increasing the G size larger than G40, the intrinsic mechanical property of G is improved. Especially, the G additive mainly anchors to one a-C surface (Figure 4d), which acts as a protective film to smooth the a-C surface and to shield the intermolecular interaction of a-C to C_8H_{16} following the slight reduction in the mobility of C_8H_{16} base oil (Figure 6a). In addition, the passivation of the friction interface is also improved (Figure 5d) and there is also no cross-linking observed. Therefore, the friction forces mainly originate from the weak intermolecular interaction between a-C and C_8H_{16}, especially the H atom in C_8H_{16} base oil,[16,25] as confirmed by Figure 3, leading to a significant reduction in the friction coefficient (Figure 2).

In region III (20−35 wt %, Figure 2) and region IV (>35 wt %, Figure 2), with the G size increased from G20 to G120, the passivation of the friction interface is improved (Figure 5d) and the diffusion coefficient of C_8H_{16} also tends to be increased because of the increased interfacial width (Figure 3) and the supporting role of the G additive (Figure 4c).[50,51] These are favorable to the sliding of the friction interface. However, under such high G content, G additives show the complicated structural evolution at the friction interface or the coexistence of different interactions with a-C and other G fragments (Figure 6c), including strong cross-linking with both the mated a-C surfaces (such as G20−46.2 wt %), coexistence of cross-linking and anchoring (such as G40−46.2 wt %), anchoring (G60−30.0 wt %), piling up (such as G91−30.2 wt %) or growth (such as G91−46.4 wt %) of G with other G fragments, and weak cross-linking with one a-C surface (such as G120−46.2 wt %). This accounts for the unregular change in the friction coefficient with G size in Figure 2.

It should be mentioned that because of the simplified friction model, the difference in friction conditions, and the difficulty in accurately tailoring the structures of graphene and a-C (roughness, fraction of dangling bonds, contamination, and so on), the direct comparison between the simulation and experiment remains a big challenge. In addition, RMD is a very time-consuming task, so in the present work, the limited number of data points (Figure 1d) is used to plot the map of the friction coefficient as a function of sizes and contents of graphene additives (Figure 2). However, this is enough to provide qualitative understanding about the dependence of the friction behavior of a-C on the graphene additive, give optimum windows of the sizes and contents of the graphene additive for achieving the low-friction behavior, and clarify the fundamental mechanism, which cannot be achieved in the experiment. The corresponding outcomes will highly accelerate the selection and design of an advanced a-C/oil/graphene synergy system for tribological applications.

4. CONCLUSIONS

In summary, at the atomic scale, we have successfully investigated the friction behavior of the a-C/liquid synergy lubricating system. The results highlight the key role of the size and content of G as an oil-based additive in the friction reduction and transformation of the interfacial structure. Main conclusions are as following.

- For each system with a fixed G size, the friction coefficient as a function G content decreases first and then increases. This mainly attributes to the transformations of the bonding state between the G additive and mated a-C surfaces and the passivation degree of the friction interface.
- However, the friction behavior exhibits more complicated evolution with G size than G content. When the G content is less than 10 wt %, the friction coefficient has no dependence on the G size. As the G content is increased to a value of 10−20 wt %, the minimal friction coefficient can be obtained for each case, but the underlying friction mechanism depends on the G size: for the G size smaller than G40, the high mobilities of the G additive and base oil improve the friction coefficient in synergism; by increasing the G size larger than G40, the G additive as a protective film smooths the friction interface by anchoring to one a-C surface, accounting for the ultralow friction coefficient combined with the decreased dangling bonds. When the excess G content (>20 wt %) is applied, the unregular change in the friction coefficient with G size is observed, which is due to the complicated structural evolution of the friction interface, especially the interactions of the G additive with a-C and other G fragments.
- This work sheds light on the effect of different sizes and contents of G additives on the friction behavior of the a-C/lubricant system and the underlying friction mechanism, which can effectively promote the commercial application of the graphene lubricant additive and develop the high-efficient a-C/lubricant system for technical and engineering applications.

■ ASSOCIATED CONTENT

Supporting Information

The Supporting Information is available free of charge at https://pubs.acs.org/doi/10.1021/acsami.0c12890.

Changes in the real contact area with size and content of the G additive. Rise of temperature with size and content of the G additive during the sliding process. Depth profiles of atomic distribution in the system. Morphology of the friction interface for the a-C@C_8H_{16} + G60−

https://dx.doi.org/10.1021/acsami.0c12890
ACS Appl. Mater. Interfaces 2020, 12, 43320−43330

12.5 wt % system after a sliding time of 1250 ps, in which the base oil molecules are neglected for view. Density of the friction interface contributed by the a-C, for a-C@C_8H_{16} + G120−22.2 wt % system. Total density of the friction interface with size and content of the G additive. Relationship between the hybridized structure and temperature at the friction interface (PDF)

AUTHOR INFORMATION

Corresponding Authors

Xiaowei Li − *School of Materials and Physics, China University of Mining and Technology, Xuzhou 221116, P. R. China; Computational Science Center, Korea Institute of Science and Technology, Seoul 136-791, Republic of Korea;* orcid.org/0000-0002-7042-2546; Phone: 82-2-958-5450; Email: lixw0826@gmail.com; Fax: 82-2-958-5451

Dekun Zhang − *School of Materials and Physics, China University of Mining and Technology, Xuzhou 221116, P. R. China*; Phone: +86 13952207958; Email: dkzhang@cumt.edu.cn

Kwang-Ryeol Lee − *Computational Science Center, Korea Institute of Science and Technology, Seoul 136-791, Republic of Korea*; Phone: 82-2-958-5494; Email: krlee@kist.re.kr; Fax: 82-2-958-5451

Author

Xiaowei Xu − *School of Physical Science and Technology, ShanghaiTech University, Shanghai 201210, P. R. China*

Complete contact information is available at: https://pubs.acs.org/10.1021/acsami.0c12890

Author Contributions

X.L., D.Z., and K.-R.L. designed the calculations. X.L. and X.X. performed the friction analysis. X.L., D.Z., and K.-R.L. cowrote the manuscript. All authors participated in the discussions and manuscript preparation.

Notes

The authors declare no competing financial interest.

ACKNOWLEDGMENTS

This work was supported by the Korea Research Fellowship Program funded by the Ministry of Science and ICT through the National Research Foundation of Korea (2017H1D3A1A01055070) and the Nano Materials Research Program through the Ministry of Science and IT Technology (NRF-2016M3A7B4025402).

REFERENCES

(1) Novoselov, K. S.; Geim, A. K.; Morozov, S. V.; Jiang, D.; Zhang, Y.; Dubonos, S. V.; Grigorieva, I. V.; Firsov, A. A. Electric Field Effect in Atomically Thin Carbon Films. *Science* **2004**, *306*, 666−669.

(2) Geim, A. K.; Novoselov, K. S. The Rise of Graphene. *Nat. Mater.* **2007**, *6*, 183−191.

(3) Geim, A. K. Graphene: Status and Prospects. *Science* **2009**, *324*, 1530−1534.

(4) Soldano, C.; Mahmood, A.; Dujardin, E. Production, Properties and Potential of Graphene. *Carbon* **2010**, *48*, 2127−2150.

(5) Liu, C.; Qiu, S.; Du, P.; Zhao, H.; Wang, L. An Ionic Liquid-Graphene Oxide Hybrid Nanomaterials: Synthesis and Anticorrosion Applications. *Nanoscale* **2018**, *10*, 8115−8124.

(6) Ren, S.; Cui, M.; Li, W.; Pu, J.; Xue, Q.; Wang, L. N-Doping of Graphene: Toward Long-Term Corrosion Protection of Cu. *J. Mater. Chem. A* **2018**, *6*, 24136−24148.

(7) Qiu, S.; Li, W.; Zheng, W.; Zhao, H.; Wang, L. Synergistic Effect of Polypyrrole-Intercalated Graphene for Enhanced Corrosion Protection of Aqueous Coating in 3.5% NaCl Solution. *ACS Appl. Mater. Interfaces* **2017**, *9*, 34294−34304.

(8) Chen, C.; Qiu, S.; Cui, M.; Qin, S.; Yan, G.; Zhao, H.; Wang, L.; Xue, Q. Achieving High Performance Corrosion and Wear Resistant Epoxy Coatings via Incorporation of Noncovalent Functionalized Graphene. *Carbon* **2017**, *114*, 356−366.

(9) Fan, X.; Wang, L. Graphene with Outstanding Anti-Irradiation Capacity as Multialkylated Cyclopentanes Additive toward Space Application. *Sci. Rep.* **2015**, *5*, 12734.

(10) Zhu, N.; Liu, W.; Xue, M.; Xie, Z.; Zhao, D.; Zhang, M.; Chen, J.; Cao, T. Graphene as a Conductive Additive to Enhance the High-Rate Capabilities of Electrospun $Li_4Ti_5O_{12}$ for Lithium-Ion Batteries. *Electrochim. Acta* **2010**, *55*, 5813−5818.

(11) Kucinskis, G.; Bajars, G.; Kleperis, J. Graphene in Lithium Ion Battery Cathode Materials: A Review. *J. Power Sources* **2013**, *240*, 66−79.

(12) Holmberg, K.; Erdemir, A. Influence of Tribology on Global Energy Consumption, Costs and Emissions. *Friction* **2017**, *5*, 263−284.

(13) Erdemir, A.; Ramirez, G.; Eryilmaz, O. L.; Narayanan, B.; Liao, Y.; Kamath, G.; Sankaranarayanan, S. K. R. S. Carbon-Based Tribofilms from Lubricating Oils. *Nature* **2016**, *536*, 67−71.

(14) Kuwahara, T.; Romero, P. A.; Makowski, S.; Weihnacht, V.; Moras, G.; Moseler, M. Mechano-Chemical Decomposition of Organic Friction Modifiers with Multiple Reactive Centres Induces Superlubricity of ta-C. *Nat. Commun.* **2019**, *10*, 151.

(15) Fan, X.; Xue, Q.; Wang, L. Carbon-Based Solid-Liquid Lubricating Coatings for Space Applications − A Review. *Friction* **2015**, *3*, 191−207.

(16) Li, X.; Wang, A.; Lee, K. R. Mechanism of Contact Pressure-Induced Friction at the Amorphous Carbon/Alpha Olefin Interface. *npj Comput. Mater.* **2018**, *4*, 53.

(17) Ye, X.; Ma, L.; Yang, Z.; Wang, J.; Wang, H.; Yang, S. Covalent Functionalization of Fluorinated Graphene and Subsequent Application as Water-Based Lubricant Additive. *ACS Appl. Mater. Interfaces* **2016**, *8*, 7483−7488.

(18) Meng, Y.; Su, F.; Chen, Y. Au/Graphene Oxide Nanocomposite Synthesized in Supercritical CO_2 Fluid as Energy Efficient Lubricant Additive. *ACS Appl. Mater. Interfaces* **2017**, *9*, 39549−39559.

(19) Ali, M. K. A.; Xianjun, H.; Abdelkareem, M. A. A.; Gulzar, M.; Elsheikh, A. H. Novel Approach of the Graphene Nanolubricant for Energy Saving via Anti-friction/Wear in Automobile Engines. *Tribol. Int.* **2018**, *124*, 209−229.

(20) Ali, M. K. A.; Xianjun, H. M50 Matrix Sintered with Nanoscale Solid Lubricants Shows Enhanced Self-lubricating Properties under Dry Sliding at Different Temperatures. *Tribol. Lett.* **2019**, *67*, 71.

(21) Chen, X.; Yin, X.; Qi, W.; Zhang, C.; Choi, J.; Wu, S.; Wang, R.; Luo, J. Atomic-Scale Insights into the Interfacial Instability of Superlubricity in Hydrogenated Amorphous Carbon Films. *Sci. Adv.* **2020**, *6*, No. eaay1272.

(22) Wang, Y.; Xu, J.; Zhang, J.; Chen, Q.; Ootani, Y.; Higuchi, Y.; Ozawa, N.; Martin, J. M.; Adachi, K.; Kubo, M. Tribochemical Reactions and Graphitization of Diamond-Like Carbon Against Alumina Give Volcano-Type Temperature Dependence of Friction Coefficients: A Tight-Binding Quantum Chemical Molecular Dynamics Simulation. *Carbon* **2018**, *133*, 350−357.

(23) Bewilogua, K.; Hofmann, D. History of diamond-like carbon films - From first experiments to worldwide applications. *Surf. Coat. Technol.* **2014**, *242*, 214−225.

(24) Robertson, J. Diamond-Like Amorphous Carbon. *Mater. Sci. Eng., R* **2002**, *37*, 129−281.

(25) Li, X.; Xu, X.; Zhou, Y.; Lee, K.-R.; Wang, A. Insights into Friction Dependence of Carbon Nanoparticles as Oil-Based Additive at Amorphous Carbon Interface. *Carbon* **2019**, *150*, 465−474.

(26) Liu, X.; Pu, J.; Wang, L.; Xue, Q. Novel DLC/Ionic Liquid/Graphene Nanocomposite Coatings towards High-Vacuum Related Space Applications. *J. Mater. Chem. A* **2013**, *1*, 3797−3809.
(27) Zhang, L.; Pu, J.; Wang, L.; Xue, Q. Frictional Dependence of Graphene and Carbon Nanotube in Diamond-Like Carbon/Ionic Liquids Hybrid Films in Vacuum. *Carbon* **2014**, *80*, 734−745.
(28) Elomaa, O.; Singh, V. K.; Iyer, A.; Hakala, T. J.; Koskinen, J. Graphene Oxide in Water Lubrication on Diamond-Like Carbon vs. Stainless Steel High-Load Contacts. *Diamond Relat. Mater.* **2015**, *52*, 43−48.
(29) Zhao, J.; Mao, J.; Li, Y.; He, Y.; Luo, J. Friction-Reduced Nano-Structural Evolution of Graphene as A Lubrication Additive. *Appl. Surf. Sci.* **2018**, *434*, 21−27.
(30) Plimpton, S. Fast Parallel Algorithms for Short-Range Molecular Dynamics. *J. Comput. Phys.* **1995**, *117*, 1−19.
(31) Li, X.; Ke, P.; Zheng, H.; Wang, A. Structure Properties and Growth Evolution of Diamond-Like Carbon FIlms with Different Incident Energies: A Molecular Dynamics Study. *Appl. Surf. Sci.* **2013**, *273*, 670−675.
(32) Li, X.; Wang, A.; Lee, K. R. Tribo-Induced Structural Transformation and Lubricant Dissociation at Amorphous Carbon/Alpha Olefin Interface. *Adv. Theory Simul.* **2019**, *2*, 1800157.
(33) Berendsen, H. J. C.; Postma, J. P. M.; van Gunsteren, W. F.; DiNola, A.; Haak, J. R. Molecular Dynamics with Coupling to an External Bath. *J. Chem. Phys.* **1984**, *81*, 3684−3690.
(34) Tavazza, F.; Senftle, T. P.; Zou, C.; Becker, C. A.; Van Duin, A. C. T. Molecular Dynamics Investigation of the Effects of Tip-Substrate Interactions during Nanoindentation. *J. Phys. Chem. C* **2015**, *119*, 13580−13589.
(35) Li, X.; Mizuseki, H.; Pai, S. J.; Lee, K.-R. Reactive Molecular Dynamics Simulation of the Amorphous Carbon Growth: Effect of the Carbon Triple Bonds. *Comput. Mater. Sci.* **2019**, *169*, 109143.
(36) Li, X.; Wang, A.; Lee, K.-R. Insights on Low-Friction Mechanism of Amorphous Carbon Films from Reactive Molecular Dynamics Study. *Tribol. Int.* **2019**, *131*, 567−578.
(37) Ma, T.-B.; Wang, L. F.; Hu, Y. Z.; Li, X.; Wang, H. A Shear Localization Mechanism for Lubricity of Amorphous Carbon Materials. *Sci. Rep.* **2014**, *4*, 3662.
(38) Ma, T.-B.; Hu, Y.-Z.; Wang, H. Molecular Dynamics Simulation of Shear-Induced Graphitization of Amorphous Carbon Films. *Carbon* **2009**, *47*, 1953−1957.
(39) Mo, Y.; Turner, K. T.; Szlufarska, I. Friction Laws at the Nanoscale. *Nature* **2009**, *457*, 1116−1119.
(40) Zilibotti, G.; Corni, S.; Righi, M. C. Load-Induced Confinement Activates Diamond Lubrication by Water. *Phys. Rev. Lett.* **2013**, *111*, 146101.
(41) Schall, J. D.; Gao, G.; Harrison, J. A. Effects of Adhesion and Transfer Film Formation on the Tribology of Self-Mated DLC Contacts. *J. Phys. Chem. C* **2010**, *114*, 5321−5330.
(42) Bai, S.; Murabayashi, H.; Kobayashi, Y.; Higuchi, Y.; Ozawa, N.; Adachi, K.; Martin, J. M.; Kubo, M. Tight-Binding Quantum Chemical Molecular Dynamics Simulations of the Low Friction Mechanism of Fluorine-Terminated Diamond-Like Carbon Films. *RSC Adv.* **2014**, *4*, 33739−33748.
(43) Xu, L.; Ma, T.-b.; Hu, Y.-z.; Wang, H. Molecular Dynamics Simulation of the Interlayer Sliding Behavior in Few-Layer Graphene. *Carbon* **2012**, *50*, 1025−1032.
(44) Bowden, F. P.; Tabor, D. *The Friction and Lubrication of Solids*; Clarendon: Oxford, 1964.
(45) Kunze, T.; Posselt, M.; Gemming, S.; Seifert, G.; Konicek, A. R.; Carpick, R. W.; Pastewka, L.; Moseler, M. Wear, Plasticity, and Rehybridization in Tetrahedral Amorphous Carbon. *Tribol. Lett.* **2014**, *53*, 119−126.
(46) Kuwahara, T.; Moras, G.; Moseler, M. Friction Regimes of Water-lubricated Diamond (111): Role of Interfacial Ether Groups and Tribo-Induced Aromatic Surface Reconstructions. *Phys. Rev. Lett.* **2017**, *119*, 096101.
(47) Mao, J.; Zhao, J.; Wang, W.; He, Y.; Luo, J. Influence of the Micromorphology of Reduced Graphene Oxide Sheets on Lubrication Properties as a Lubrication Additive. *Tribol. Int.* **2018**, *119*, 614−621.
(48) Fan, K.; Chen, X.; Wang, X.; Liu, X.; Liu, Y.; Lai, W.; Liu, X. Toward Excellent Tribological Performance as Oil-Based Lubricant Additive: Particular Tribological Behavior of Fluorinated Graphene. *ACS Appl. Mater. Interfaces* **2018**, *10*, 28828−28838.
(49) Li, X.; Wang, A.; Lee, K.-R. Atomistic Understanding on Friction Behavior of Amorphous Carbon Films Induced by Surface Hydrogenated Modification. *Tribol. Int.* **2019**, *136*, 446−454.
(50) Lin, J.; Wang, L.; Chen, G. Modification of Graphene Platelets and Their Tribological Properties as a Lubricant Additive. *Tribol. Lett.* **2011**, *41*, 209−215.
(51) Xiao, H.; Liu, S. 2D Nanomaterials as Lubricant Additive: A Review. *Mater. Des.* **2017**, *135*, 319−332.
(52) Gao, G. T.; Mikulski, P. T.; Harrison, J. A. Molecular-Scale Tribology of Amorphous Carbon Coatings: Effects of Film Thickness, Adhesion, and Long-Range Interactions. *J. Am. Chem. Soc.* **2002**, *124*, 7202−7209.
(53) Li, X.; Wang, A.; Lee, K.-R. Transformation of Amorphous Carbon to Graphene on Low-Index Ni Surfaces during Rapid Thermal Processing: A Reactive Molecular Dynamics Study. *Phys. Chem. Chem. Phys.* **2019**, *21*, 2271−2275.

https://dx.doi.org/10.1021/acsami.0c12890
ACS Appl. Mater. Interfaces 2020, 12, 43320−43330